Silicon vacancy-related centers in non-irradiated $6H$-SiC nanostructure

© N.T. Bagraev[¶+*], E.Yu. Danilovskii[+], D.S. Gets[+], E.N. Kalabukhova[‡], L.E. Klyachkin[+],
  A.A. Koudryavtsev[+], A.M. Malyarenko[+], V.A. Mashkov[*],
  D.V. Savchenko[‡•], B.D. Shanina[‡]

[+] Ioffe Physicaltechnical Institute, Russian Academy of Sciences,
194021 St. Petersburg, Russia
[*] State Polytechnical University,
195251 St. Petersburg, Russia
[‡] Lashkaryov Institute of Semiconductor Physics, National Academy of Sciences of Ukraine,
03028 Kyiv, Ukraine
[•] Institute of Physics, Academy of Sciences of Czech Republic,
Praha, Czech Republic

We present the first findings of the silicon vacancy related centers identified in the non-irradiated 6H-SiC nanostructure using the electron spin resonance (ESR) and electrically-detected (ED) ESR technique. This planar 6H-SiC nanostructure represents the ultra-narrow p-type quantum well confined by the δ-barriers heavily doped with boron on the surface of the n-type 6H-SiC (0001) wafer. The new EDESR technique by measuring the only magnetoresistance of the 6H-SiC nanostructure under the high frequency generation from the δ-barriers appears to allow the identification of the isolated silicon vacancy centers as well as the triplet center with spin state $S = 1$. The same triplet center that is characterized by the large value of the zero-field splitting constant D and anisotropic g-factor is revealed by the ESR (X-band) method. The hyperfine (HF) lines in the ESR and EDESR spectra originating from the HF interaction with the ^{14}N nucleus seem to attribute this triplet center to the N$-V_{Si}$ defect.

1. Introduction

Recently the N$-V_{Si}$ ($S = 1$) defect in the diamond, silicon carbide 4H- and 6H-SiC structures became to be of interest as a qubit for quantum computing operations owing to the possibility to control the coherent spin processes at room temperature [1–5]. However, up to now the N$-V_{Si}$ defect and other silicon vacancy related centers were introduced into these wide gap semiconductors only by the neutron, proton and electron irradiation with subsequent thermal annealing. Therefore the preparation of samples containing the only N$-V_{Si}$ defects and isolated silicon vacancies for the realization of the qubit versions has been always difficult because of the different defects created under this irradiation which are able to give rise to the non-radiative recombination.

In present work we demonstrate the results of the electron spin resonance (ESR) and electrically-detected (ED) ESR studies of the N $- V_{Si}$ defect and the isolated silicon vacancy centers which are formed in the course of preparation of the planar 6H-SiC nanostructure without any previous or subsequent electron (e) and neutron (n) irradiation. The new EDESR technique used here allows the identification of point and extended defects by measuring the only magnetoresistance without application of an external cavity as well as a hf source and recorder, with internal high frequency generation within frameworks of the normal-mode coupling (NMC) caused by the microcavities embedded in a semiconductor nanostructure [6].

¶ E-mail: Impurity.Dipole@mail.ioffe.ru

2. Results

The device has been prepared within frameworks of the planar technology on the n-type 6H-SiC (0001) wafer doped with nitrogen at the concentration of $5 \cdot 10^{18}$ cm^{-3}. Firstly, the pyrolysis of silane was used to obtain the oxide overlayer on the 6H-SiC (0001) surface. Then, the photolithography processes and subsequent etching were applied to make the Hall geometry windows (see Fig. 1, a). Finally, the short-time diffusion of boron has been performed from the gas phase under controlled injection of the silicon vacancies at the temperature of $T = 900°$C [7]. The shallow diffusion profiles of boron were measured using the SIMS (secondary ion mass spectrometry) technique that has revealed the important role of the low temperature dissociative vacancy diffusion mechanism due to excessive amount of the silicon vacancies generated by the 6H-SiC$-$SiO$_2$ interface (Fig. 2, a).

The quantum conductance and tunneling spectroscopy measurements have shown that the p^+-diffusion profile obtained represents the ultra-narrow p-type quantum well (QW) confined by the δ-barriers heavily doped with boron, concentration N(B) $> 10^{21}$ cm^{-3} [7]. Moreover, the negative differential resistance appeared to be observed under the voltage applied both to the p^+-n junction and along the device thereby verifying the correlation gap in the one-electron band scheme of the δ-barriers (see Fig. 3, a). This correlation gap as well as the fall in the electrical activity of shallow boron acceptors contrary to high level of boron doping seems to result from the negative-U reconstruction, 2B$^0 \rightarrow$ B$^+ +$ B$^-$ along the **c**-axis (Figs. 1, b and 2, b).

Figure 1. a — Device schematic, showing the perspective view of the 6H-SiC nanostructure performed within the frameworks of the Hall geometry; the 6H-SiC nanostructure represents the p-type 6H-SiC quantum well confined by the δ-barriers heavily doped with boron on the n-type 6H-SiC surface; the changes of the longitudinal, U_{xx}, and the transverse, U_{xy}, voltage are measured by varying the value of the external magnetic field when the drain−source current, I_{ds}, is stabilized at the extremely low value. b — Silicon carbide polytype 6H-SiC.
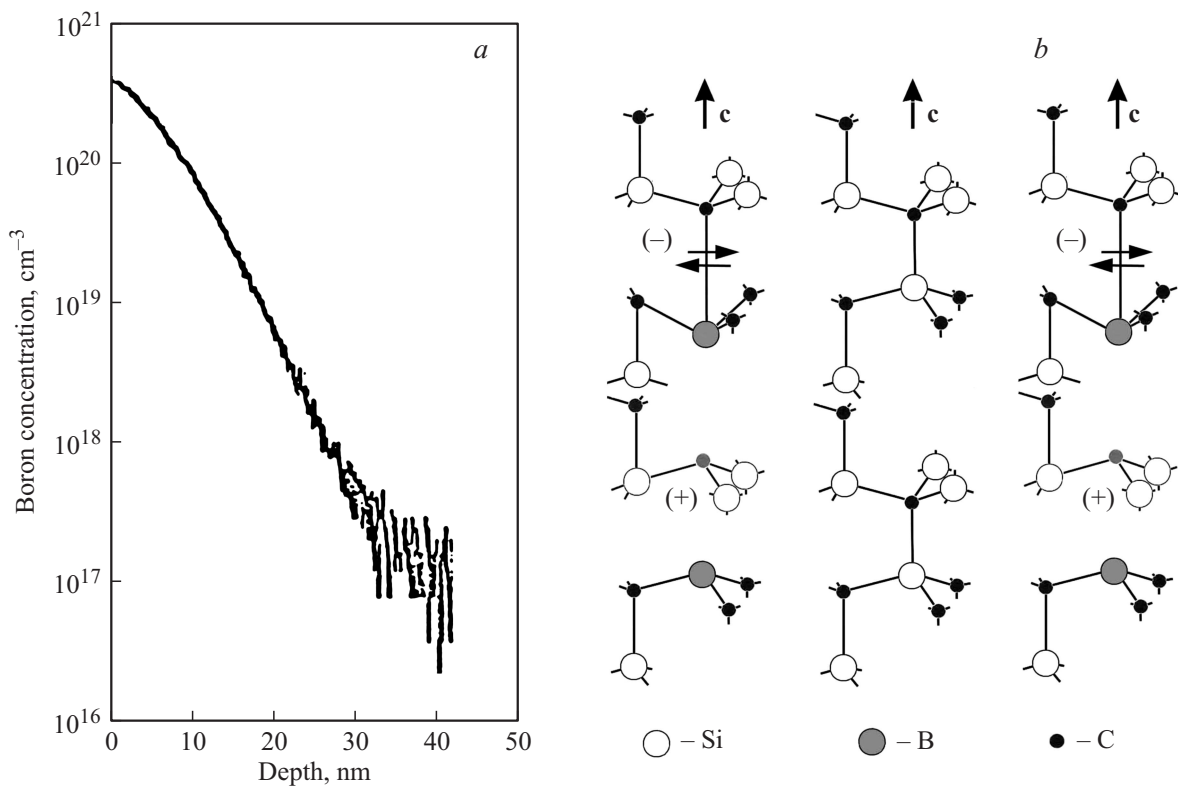
Figure 2. a — SIMS data for the p^+-boron diffusion profile on the n-type 6H-SiC (0001) surface; the short-time diffusion of boron has been performed under controlled injection of silicon vacancies at the temperature of 900°C after previous oxidation using the pyrolysis of silane. b — Negative-U dipole boron centers in 6H-SiC; $2B^0 \rightarrow B^+ + B^-$.

It should be noted that the dipole boron centers in 6H-SiC similarly to the trigonal $B^+ + B^-$ pairs in silicon appeared to be the effective internal broadband source of the GHz and THz emission, with the frequency selection dependent on the characteristics of the n-type 6H-SiC substrate as a load resistance (see Fig. 3, b) [6,8]. Therefore
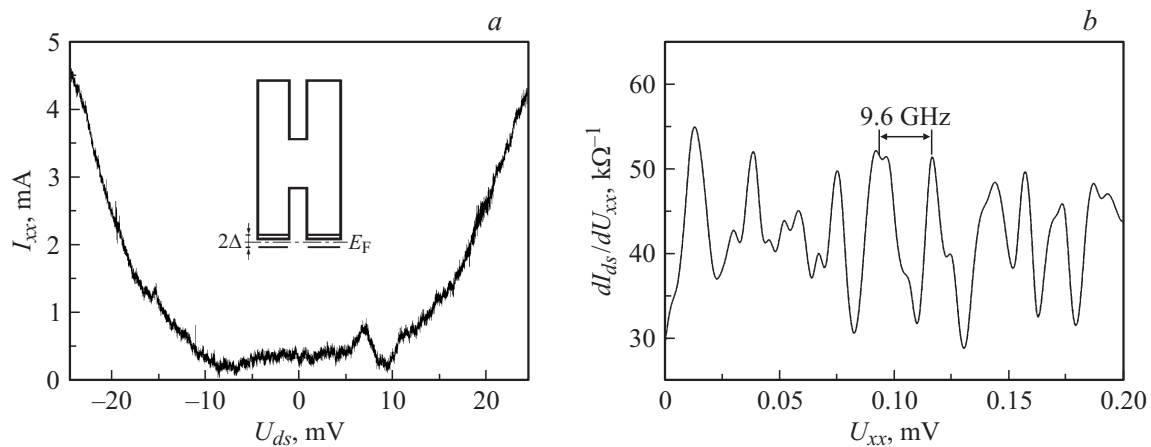
Figure 3. Correlation energy gap in the one-electron band scheme of the 6H-SiC nanostructure that represents the p-type 6H-SiC quantum well confined by the δ-barriers heavily doped with boron on the n-type 6H-SiC surface. a — The correlation energy gap in the valence band of the δ-barriers which is caused by forming the negative-U dipole boron centers, $2B^0 \rightarrow B^+ + B^-$, is revealed by measuring the longitudinal current–voltage characteristics, $I_{xx} = f(U_{ds})$, as a function of the positive and the negative values of drain–source voltage, U_{ds}, at the temperature of 77 K; the insert shows the one-electron band scheme of the 6H-SiC nanostructure with the correlation gap near the valence band of the δ-barriers. b — The oscillating dependence $dI_{ds}/dU_{xx} = f(U_{xx})$ that was measured by varying the values of the stabilized drain–source current at the temperature of 77 K appears to result from the GHz emission due to the excitation of the dipole boron centers in the δ-barriers; the frequency selection at the value of 9.6 GHz was used by varying the value of a load resistance and by incorporating the microcavities in the plane of the 6H-SiC nanostructure.

the δ-barriers heavily doped with boron substantially promote the electrically and optically detected ESR (EDESR and ODMR, respectively) techniques without application of the external hf source in low-dimensional semiconductor structures [6,9–12]. In this case the internal hf emitter is able to excite the transitions between Zeeman sublevels of free carriers and single point defects under both drain–source and the p^+-n junction bias voltages, thereby making possible the ESR measurements as the response of conductance or luminescence by varying the external magnetic field. Besides, to enhance the sensitivity of the EDESR and ODMR techniques, the special microcavities were incorporated into the plane of a nanostructure, with the sizes corresponding to the frequencies, $L = \lambda/2n$, where n is the refractive index, L is the microcavity size and λ is the wavelength of the GHz and THz radiation. Here the length of the δ-barrier area was picked up to satisfy to the selection of the frequency value of 9.6 GHz.

When inserted in a microcavity, the hf excited Zeeman system with two or more sublevels can be revealed in a weak or strong coupling regime. For weak coupling, the amplitude of ESR spectra can be enhanced or reduced by tuning the discrete microcavity modes in and out resonance conditions. By contrast, strong coupling is characterized by the reversible energy exchange between the microcavity mode and the hf induced Zeeman transitions, which is expected to result in the Rabi splitting in the ESR (EDESR and ODMR) spectra. This coherent coupling seems to be an analogue of well-known normal-mode coupling (NMC) regime caused by the microcavities embedded in a semiconductor nanostructure that is revealed by measuring a Rabi splitting in optical spectra as a consequence of anti-

crossings between the quantum dot exciton and microcavity-mode dispersion relations [13].

In addition to the aforesaid, the contribution to the internal hf generation seems to be caused by the spin precession of the $B^+ + B^-$ dipole moment that results in the Rabi oscillations and by the spin-dependent hole scattering on the negative-U dipole boron centers that appears to induce the Bloch oscillations. Besides, in the case of homogeneous distribution of the dipole boron centers, the δ-barriers have been shown to exhibit the properties of high temperature superconductors. Therefore the internal hf generation seems to result from the Josephson emission, with the frequency selection controlled by measuring the Shapiro steps [6].

Thus, the GHz emission from the δ-barriers appeared to be a basis of the new EDESR technique by measuring the dependences of the longitudinal, U_{xx}, and transverse, U_{xy}, voltages on the magnetic field value without an external hf source and a recorder as well as the external cavity [6]. Here this EDESR technique was used to identify the silicon vacancy related centers in the planar 6H-SiC nanostructure that was not exposed to previous or subsequent e- and n-irradiation. Finally, contrary to minor amounts of centers, the $N-V_{Si}$ defect was identified for the first time in the planar 6H-SiC nanostructure with the ESR Bruker ELEXSYS E580 spectrometer at 9.7 GHz in the temperature interval from $T = 5$ to 40 K.

3. Discussion

The EDESR spectra of the isolated silicon vacancy centers that have been formed in the process of the preparation
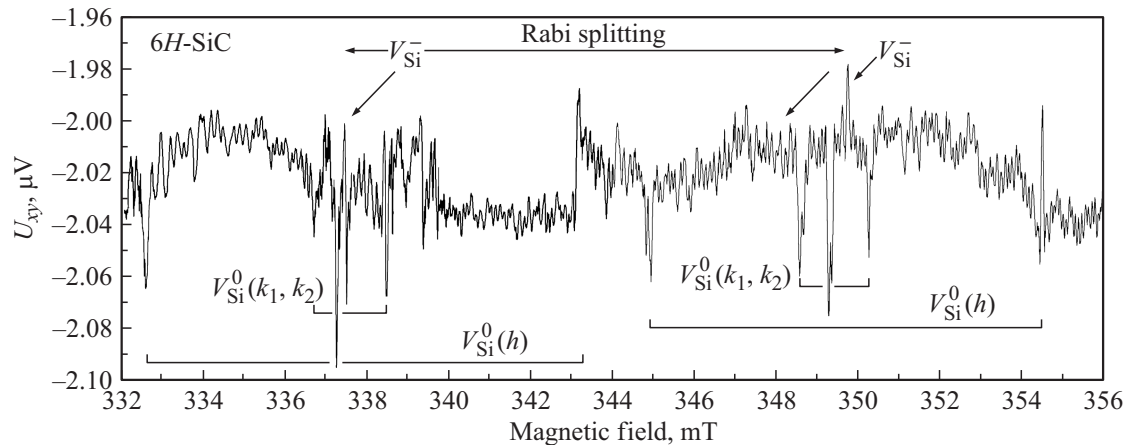
Figure 4. The EDESR spectra of the isolated silicon vacancy centers in the p-type $6H$-SiC QW confined by the δ-barriers heavily doped with boron on the n-type $6H$-SiC (0001) surface, which was observed by measuring the only Hall magnetoresistance without the external cavity as well as the external hf source and recorder. $\mathbf{B} \parallel \mathbf{c}$, $T = 77$ K, the frequency of the internal hf generation was equal to $\nu = 9.6$ GHz, and the drain−source current was stabilized at the value of $I_{ds} = 10$ nA. The Rabi splitting is demonstrated, which is attributed to the normal-mode coupling (NMC) with the isolated vacancy center embedded in the microcavity that is incorporated in the $6H$-SiC planar nanostructure.
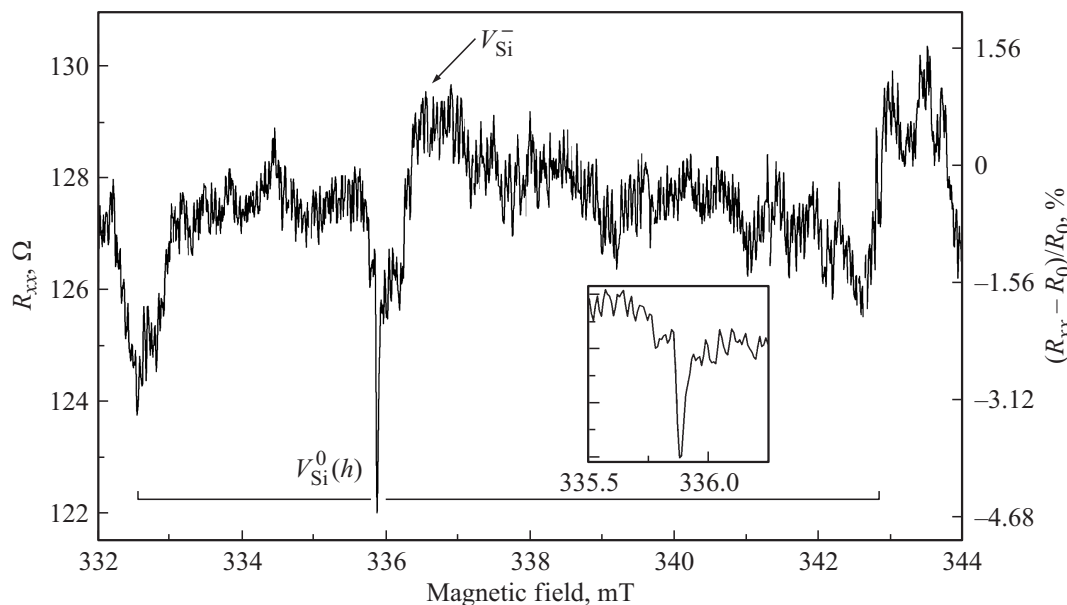
Figure 5. The EDESR spectra of the isolated silicon vacancy centers in the p-type $6H$-SiC QW confined by the δ-barriers heavily doped with boron on the n-type $6H$-SiC (0001) surface, which was observed by measuring the only longitudinal magnetoresistance without the external cavity as well as the external hf source and recorder. $\mathbf{B} \parallel \mathbf{c}$, $T = 77$ K, the frequency of the internal hf generation was equal to $\nu = 9.6$ GHz, and the drain−source current was stabilized at the value of $I_{ds} = 10$ nA. The EDESR spectrum of residual shallow boron centers in the $6H$-SiC nanostructure is shown in insert.

of the $6H$-SiC planar nanostructure are shown in Figs. 4 and 5. These spectra were observed by measuring the only longitudinal or Hall magnetoresistance without the external cavity as well as the external hf source and recorder at the temperature of $T = 77$ K, in the geometry of the magnetic field $\mathbf{B}$ and crystallographic axic $\mathbf{c}$ $\mathbf{B} \parallel \mathbf{c}$, the frequency of the internal hf generation was equal to $\nu = 9.6$ GHz, and the drain−source current was stabilized at the value of $I_{ds} = 10$ nA. The Rabi splitting is demonstrated when

the field dependent U_{xy} voltage is registered, which is attributed to the normal-mode coupling (NMC) with the isolated vacancy center embedded in the microcavity that is incorporated in the $6H$-SiC planar nanostructure. The lack of the Rabi splitting in the EDESR spectrum observed by measuring the U_{xx} voltage seems to be evidence of very high sensitivity of the strong coupling regime to the relation between the coherence length and the mutual arrangements of contact areas. The role of the edge channels
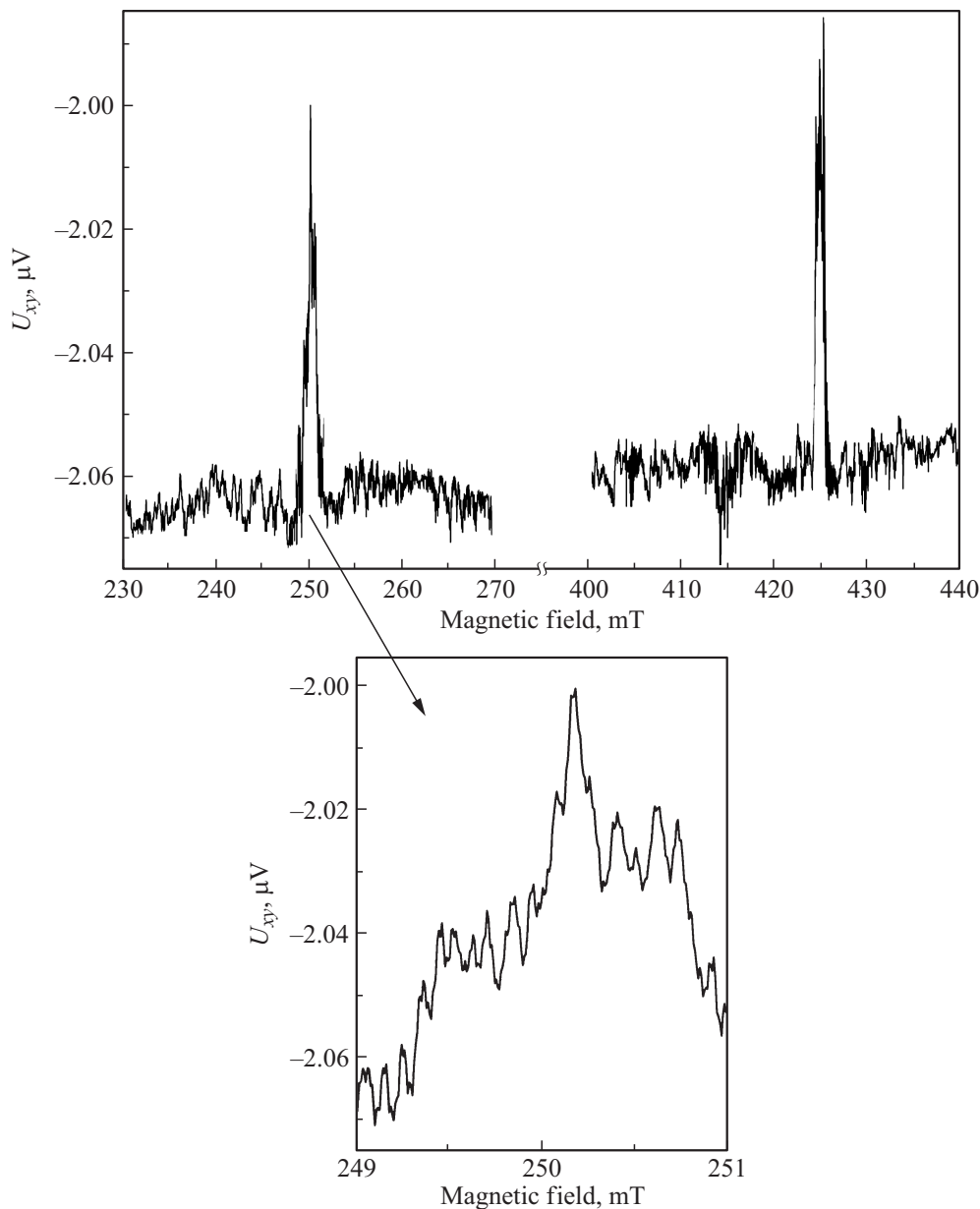
Figure 6. The EDESR spectrum of the $N-V_{Si}$ defect ($S = 1$) observed in the *p*-type 6*H*-SiC QW confined by the δ-barriers heavily doped with boron on the *n*-type 6*H*-SiC (0001) surface, which was observed by measuring the only Hall magnetoresistance without the external cavity as well as the external hf source and recorder. $\mathbf{B} \parallel \mathbf{c}$, $T = 77$ K. The frequency of the internal hf generation was equal to $\nu = 9.6$ GHz, and the drain−source current was stabilized at the value of $I_{ds} = 10$ nA. Fine structure resolved in the EDESR spectrum appears to be evidence of the nitrogen presence ($I = 1$). Isolated nitrogen donor centers inside the 6*H*-SiC nanostructure were absent as a result of interaction with silicon vacancies that seems to give rise to the formation of the $N - V_{Si}$ defects.

in the relative contribution of the weak and strong coupling to the EDESR signal is also needed to be taken into account.

The EDESR spectra shown in Figs. 4 and 5 appear to be in a good agreement with the data obtained by the *X*-band ESR and EDESR standard methods in the studies of the isolated silicon vacancy centers created under *e*-irradiation in the 6*H*-SiC bulk sample [14–16]. In particular, the central line in Figs. 4 and 5 marked by V_{Si}^- is attributed to the negatively charged silicon vacancy with $S = 3/2$, whereas

the lines indicated by $V_{Si}^0(h)$ and $V_{Si}^0(k_1, k_2)$ are related to the neutral charge silicon vacancy but in different positions in the crystalline lattice. Symbols „h" and „k_1, k_2" depict the hexagonal and the quasi-cubic positions in the 6*H*-SiC crystal that has a hexagonal symmetry with the symmetry axis **c** (see Figs. 1, *b* and 2, *b*). It should be noted that the different phase of the lines from the triplet $V_{Si}^0(h)$ center is evidence of non-equilibrium spin polarization that seems to be caused by the hf pumping from the δ-barriers heavily doped with boron.
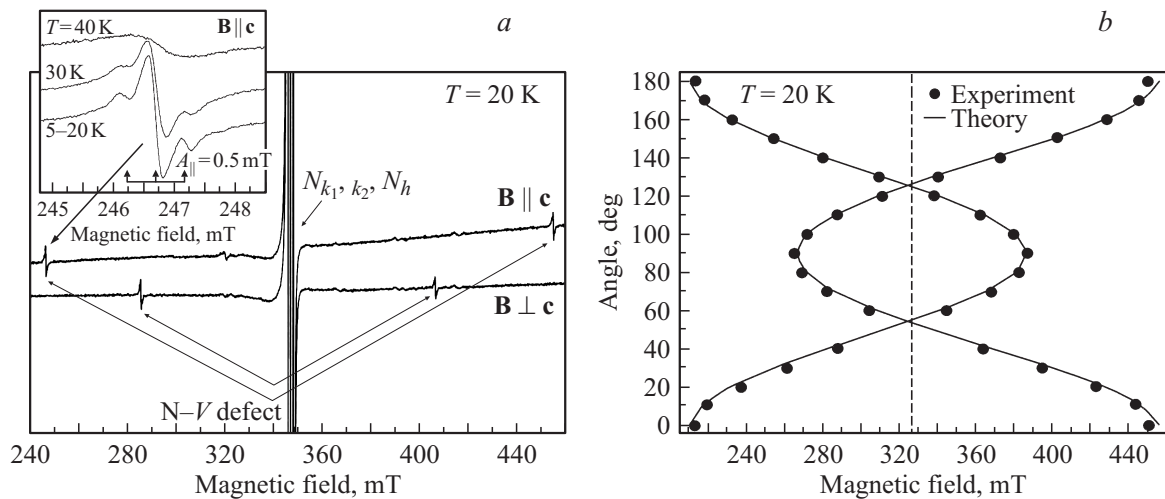
Figure 7. The ESR spectrum (*a*) and the angular dependence of the fs structure constant D (*b*) of the triplet center observed in the *p*-type 6*H*-SiC QW confined by the δ-barriers heavily doped with boron on the *n*-type 6*H*-SiC (0001) surface. *a* — The fine structure resolved in the ESR spectrum of a triplet center is shown in insertion. *b* — The rotation of the magnetic field was in $(11\overline{2}0)$ plane. $T = 20\,\mathrm{K}$.

The presence of the residual shallow boron centers in the EDESR spectrum are also worthy of notice, because the most boron dopants are involved in the formation of the negative-*U* dipole boron centers (see Figs. 4 and 5). This result appears to highlight the high sensitivity of the EDESR method used in both strong and weak coupling regimes which allows the identification of the single centers in semiconductor nanostructures. Since the measurements of the magnetoresistance were performed without any light illumination and injection of carriers from the contacts, the spin-dependent scattering of spin-polarized holes on the paramagnetic centers in the edge channels of the 6*H*-SiC planar nanostructure appear to underlie the mechanism of the EDESR method, with internal hf emission in the presence of a microcavity [6]. Therefore the EDESR sensitivity determined by the magnetoresistance response appears to be interpreted here in terms of the interference transition in the diffusive transport of free holes respectively between the weak anti-localization regime $(\tau_S > \tau_\varphi > \tau_m)$ in the region far from the ESR of a paramagnetic point defect located inside the edge channel and the weak localization regime $(\tau_\varphi > \tau_S > \tau_m)$ in the nearest region of the ESR of that defect [6]. It follows that the important condition to register this resonant magnetoresistance response is to stabilize the drain−source current at the value lower than 10 nA, which provides the spin interference regimes in the edge channels. Except the aforesaid it is necessary to pay attention that the EDESR spectra shown in Figs. 4 and 5 were observed at the temperature of 77 K. This unusual result seems to be a consequence of sharp increase in the spin−lattice relaxation time of holes in the low-dimensional silicon structures [6,11,12]. Besides, the strong anisotropy of the spin–lattice relaxation time seems to result in the disappearance of the $V_{\mathrm{Si}}^0(k_1, k_2)$ lines in the EDESR spectrum registered by measuring the field dependent U_{xx} voltage (see Fig. 5).

The EDESR spectrum of the triplet N−V_{Si} defect $(S = 1)$ consists of two strong lines located at 250 and 450 mT (see Fig. 6). The high resolution of the EDESR method allowed the registration of the N−V_{Si} defect fine structure as a result of which the lines of spectra are divided into three lines due to nitrogen nuclear spin $I = 1$, with the value of the hf splitting equal to 0.5 mT. The absence of the EDESR lines related to the nitrogen donor center is of importance to be noticed, which seems to result from the capture of silicon vacancies practically all of them in the area of the quantum well confined by the δ-barriers heavily doped with boron. Besides, the sensitive volume of the EDESR method is about several nanometers in the depth of the sample multiplied by Hall bar geometry area of the device structure that hinders from the identification of defects in the volume of the *n*-type 6*H*-SiC (0001) wafer. However the EDESR method based on the registration of the negative or positive magnetoresistance in the weak localization regime under resonance conditions is highly sensitive inside the QW area [6]. In particular, the EDESR spectrum of the N−V_{Si} defect shown in Fig. 6 reflects the contribution from $5 \cdot 10^4$ centers taking account of the section area of the edge channels in the device structure, 2×2 nm, while the ordinary ESR method allows signal detection minimum from 10^{10} spins.

This value corresponds to the maximum number of the N−V_{Si} defects which can be created by the capture of silicon vacancies on nitrogen donors in the process of the preparation of the device if to take into account the sizes of the doping area. This important condition allowed the ESR detection of the N−V_{Si} defects in the same device with the highly sensitive Bruker ELEXSYS E580 spectrometer (see Fig. 7, *a*).

In addition to the dominant spectrum of the nitrogen (N) donors substituting quasi-cubic (N_{k_1,k_2}) and hexagonal (N_h) sites originated from the *n*-type 6*H*-SiC (0001) bulk
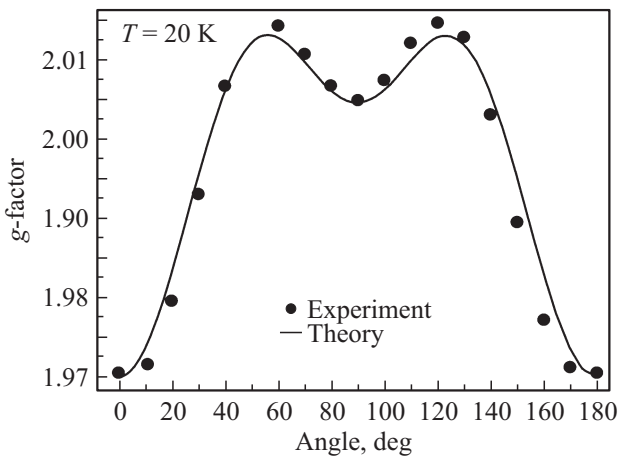
Figure 8. Angular dependence of the $g_{\text{eff}}(\theta)$ obtained from experiment and theory.

area, a fine structure (fs) doublet lines of small intensity with fs splitting of $\Delta B_{\parallel} = 237.6\,\text{mT}$ is observed in the temperature interval from 5 to 40 K and is related to the triplet center with $S = 1$. The fact that the fs lines corresponding to the electron transitions ($M_S = 1 \rightarrow M_S = 0$; $M_S = -1 \rightarrow M_S = 0$) were detected in darkness confirms a triplet ground state of the defect center. When the amplitude modulation of the magnetic field was taken smaller than the width of the triplet lines, as can be seen from Fig. 7, *a*, three hyperfine (HF) lines can be well resolved in the ESR spectrum of the defect center with value of the HF splitting of $\sim 0.5\,\text{mT}$. The presence of the three HF lines indicates its origin from the HF interaction with one ^{14}N nuclei ($S = 1/2$ and $I = 1$). Thus, triplet center seems to consist of the nitrogen atom and silicon vacancy introduced into the device in the process of its preparation. Since there are three nonequivalent positions for the impurities and defects in the 6*H*-SiC lattice, it is expected that this property is also attributed to the observed defect. Therefore different intensities of the central HF triplet line and sidelines in Fig. 7, *a* can be explained by the contribution of the ESR spectrum due to the defect substituting a hexagonal site in the central line, which has a smaller unresolved HF structure. From the ratio between the central and side lines of the nitrogen triplet, it was concluded that the triplet with the HF splitting of the 0.5 mT value corresponds to the defect substituting one quasi-cubic position. The angular dependence of the ESR spectrum shown in Fig. 7, *b* that was measured by the rotation of the magnetic field in the plane inclusive the **c** axis appears to demonstrate the angular variation characteristic for a spin $S = 1$ center.

The experimental angular dependence of the effective g-factor of ESR spectrum one can obtain taking the half-sum of the resonance fields of two spectral components: $g_{\text{eff}}(\theta) = 2h\omega_0/\beta(H_{-1} + H_{+1})$, where $g_{\text{eff}}(\theta)$ is an effective anisotropic g-factor of the center, H_{-1}, H_{+1} are the low-field and high-field components of the resonance field of ESR spectrum; ω_0 is the microwave field frequency. The obtained experimental angular dependence $g_{\text{eff}}(\theta)$ plotted

in Fig. 8 is described by the following expression:

$$g_{\text{eff}}(\theta) = 1.999 - 0.0174\cos(2\theta) - 0.0124\cos(4\theta). \quad (1)$$

The difference between the function describing the experimental curve in Fig. 8 and the axially symmetric angular dependence of the g-factor expressed by $g = (g_{\parallel}\cos^2\theta + g_{\perp}\sin^2\theta)^{1/2}$ arises from the last term in Eq. (1). Because of the large value of the fs splitting it was suggested that the second order of the crystalline field contributes into this term. Ignoring the term describing the HF interaction the spin Hamiltonian for the paramagnetic $S = 1$ center with axial crystalline field D and axial g-tensor ($g_{\parallel}$, $g_{\perp}$) is described as

$$\hat{H} = g_{\parallel}H_z S_z + g_{\perp}(H_x S_x + H_y S_y) + D\left(S_z^2 - S(S+1)/3\right). \quad (2)$$

Since the crystal-field term is large, to analyze the parameters of the triplet center the direct numerical diagonalization of the spin-Hamiltonian matrix was required. To this end the laboratory axes system was rotated so that the spin Hamiltonian may be written in a diagonal form in the applied magnetic field $B_0 = (0, \sin\theta, \cos\theta)$:

$$\hat{H} = gH_{z'}S_{z'} + D_0\left[S_{z'}^2 - S(S+1)/3\right]$$
$$- D_1\left[S_z(S_+ + S_-) + (S_+ + S_-)S_z\right] + D_2\left(S_+^2 + S_-^2\right)/2,$$
$$D_0 = 0.5D\left[3g_{\parallel}^2\cos^2(\theta)/g^2 - 1\right],$$
$$g^2 = g_{\parallel}^2\cos^2(\theta) + g_{\perp}^2\sin^2(\theta),$$
$$D_1 = Dg_{\parallel}g_{\perp}\sin(2\theta)/(4g^2), \quad D_2 = Dg_{\perp}^2\sin^2(\theta)/g^2. \quad (3)$$

Then the secular equation for the eigenvalues of the $\hat{H}$ on the spin wave functions $|-1\rangle$, $|0\rangle$, $|1\rangle$ is given by

$$\begin{vmatrix} g(\theta)H + D_0 - \varepsilon & d_1 & d_2 \\ d_1 & -\varepsilon & -d_1 \\ d_2 & -d_1 & -g(\theta)H + D_0 - \varepsilon \end{vmatrix} = 0 \quad (4)$$

where

$$d_1 = Dg_{\parallel}g_{\perp}\sin(2\theta)/(2\sqrt{2}g^2),$$
$$d_2 = 0.5D(g_{\perp}^2/g^2)\sin^2(\theta).$$

Solving Eq. (4) at an angle of $\theta = 0$, we have found the constant of the crystalline field $D = 120\,\text{mT}$ and $g_{\parallel} = 1.9700$. For the case of $\theta = 90°$, $d_1 = 0$, $d_2 = 0.5D$ the solution of Eq. (4) yields $g_{\perp} = 1.9964$. With the values of $g_{\parallel}$, $g_{\perp}$, D the angular dependence of the g-factor for arbitrary angle θ can be obtained by the numerical calculation of the cubic equation derived from Eq. (4):

$$\varepsilon^3 - a\varepsilon^2 - b\varepsilon - c = 0 \quad (5)$$

where $a = 2D_0$, $b = (g^2H_{\text{res}}^2 + d_2^2 + 2d_1^2 - D_0^2)$, $c = 2D_0d_1^2 + 2d_1^2d_2$.

Because of the large value of the crystalline field constant D, the constant c in Eq. (5) cannot be neglected and

Parameters of the spin Hamiltonian for triplet centers observed in the 6*H*-SiC nanostructures, *e*-irradiated synthetic bulk diamond and *n*-irradiated bulk 6*H*-SiC of the *n*-type

Center	S	T, K	g-factor	A, mT	D, 10^{-4} cm^{-1}	References
N$-V$ (diamond *e*-irradiated)	1		$g = 2.0028$	$A_{\parallel} = 0.082$ $A_{\perp} = 0.075$	960.7	[17]
N$_C-V_{Si}$ (6*H*-SiC *n*-irradiated)	1	3.5 70	$g = 2.003$	$A_{\parallel} = 0.55$ $A_{\parallel} = 0.75$ $A_{\perp} = 0.35$	860 885	[18]
N$_C-V_{Si}$ (6*H*-SiC nanostructure)	1	5$-$40	$g_{\parallel} = 1.9700(3)$ $g_{\perp} = 1.9961(3)$	$A_{\parallel} = 0.55$ $A_{\perp} = 0.45$	1140	This work

the result of numerical calculation for $g_{\rm eff}(\theta) = \omega_0/(\beta H_{\rm res})$, shown in Fig. 7, *b* by the solid line, indicates that the term proportional to $\cos(4\theta)$ in Eq. (1) arises from constant *c*. The parameters of the triplet center obtained from numerical diagonalization of the spin Hamiltonian are given in Table.

For comparison, the parameters of the N$-V_{Si}$ triplet centers containing in their structure nitrogen atoms which were observed previously in electron irradiated (dose $10^{12}-10^{15}$ cm^{-2}) and annealed at 900°C synthetic diamond and in neutron irradiated (dose 10^{21} cm^{-2}) *n*-type 6*H*-SiC after high temperature annealing at 2000°C are listed in Table.

As can be seen from Table, the observed triplet centers have close values of the fs splitting constants and were attributed to the defect center formed between nitrogen atom and vacancy. The triplet center observed in the 6*H*-SiC nanostructure has larger fs constant than that observed in irradiated synthetic diamond and 6*H*-SiC. At the same time the hf splitting due to the interaction with ^{14}N nucleus has the same value as for the triplet center observed in the *n*-irradiated 6*H*-SiC at the temperature of 5 K. Taking into account that silicon vacancy (V_{Si}) is more mobile at the temperature of 900°C than the carbon vacancy (V_C) and appears to dominate as a carrier in the process of low temperature impurity diffusion into the *n*-type 6*H*-SiC bulk samples, the observed triplet center was also attributed to the N$-V_{Si}$ related center.

4. Conclusions

The electron spin resonance (ESR) and electrically-detected (ED) ESR studies have been shown to the isolated silicon vacancy and N$-V_{Si}$ defect that are formed during the preparation of the planar nanostructures under the conditions of the silicon vacancy injection from the SiO$_2$/*n*-6*H*-SiC interface without any previous and subsequent irradiations. This planar 6*H*-SiC nanostructure represents the ultra-shallow quantum well of the *p*-type confined by the δ-barriers heavily doped with boron on the *n*-6*H*-SiC surface, which are self-assembled under oxidation process and subsequent short-time diffusion of boron. The EDESR measurements of the point defects in planar 6*H*-SiC nanostructures have been proved within frameworks of the

Hall geometry by measuring the only magnetoresistance without the external cavity as well as the hf source and recorder owing to the microcavities embedded in the QW plane and internal hf generation from the δ-barriers heavily doped with boron. The EDESR spectrum of the isolated silicon vacancy revealed both negative state ($S = 3/2$) and the neutral $V_{Si}(h)$, $V_{Si}(k_1, k_2)$ states ($S = 1$). Besides, $N-V_{Si}$ defect has been found by both the EDESR method at the temperature of 77 K and the ESR (*X*-band) method with the high sensitive ESR spectrometer Bruker ELEXSYS E580 in the temperature interval from 5 to 40 K, with demonstration of very identical spectra of the triplet center ($S = 1$). The hyperfine lines in the ESR and EDESR spectra originating from the HF interaction with the ^{14}N nucleus seem to attribute this triplet center to the N$-V_{Si}$ defect.

The N$-V_{Si}$ spectrum characterized by the splitting value equal to $\Delta B = 237.6$ mT has been observed using the ESR (*X*-band) technique however with the nitrogen ESR spectrum corresponding to the nitrogen concentration in the *n*-type 6*H*-SiC bulk crystal, $5 \cdot 10^{18}$ cm^{-3}, whereas the EDESR spectrum revealed no nitrogen centers, because of the full occupation by silicon vacancies inside the planar 6*H*-SiC nanostructure.

Finally, the striking result obtained in this work is that in distinction from the known N$-V_{Si}$ defects observed in the *e*-irradiated diamond and in the heavy *n*-irradiated and high temperature annealed *n*-type 6*H*-SiC, the N$-V_{Si}$ center characterized by the larger value of the zero-field splitting constant *D* and anisotropic *g*-factor was found in the non-irradiated 6*H*-SiC nanostructure.

References

[1] V. Jacques, P. Neumann, J. Beck, M. Markham, D. Twitchen, J. Meijer, F. Kaiser, G. Balasubramanian, F. Jelezko, J. Wrachtrup. Phys. Rev. Lett., **102**, 057 403 (2009).

[2] P.G. Baranov, A.A. Soltamova, D.O. Tolmachev, N.G. Romanov, R.A. Babunts, F.M. Shakhov, S.V. Kidalov, A.Y. Vul', G.V. Mamin, S.B. Orlinskii, N.I. Silkin. Small, **7**, 1533 (2011).

[3] D. Riedel, F. Fuchs, H. Kraus, S. Väth, A. Sperlich, V. Dyakonov, A.A. Soltamova, P.G. Baranov, V.A. Ilyin, G.V. Astakhov. Phys. Rev. Lett., **109**, 226 402 (2012).

[4] P. London, J. Scheuer, J.-M. Cai, I. Schwarz, A. Retzker, M.B. Plenio, M. Katagiri, T. Teraji, M. Koizumi, J. Isoya, R. Fischer, L.P. McGuinness, B. Naydenov, F. Jelezko. Phys. Rev. Lett., **111**, 067 601 (2013).

[5] H. Kraus, V.A. Soltamov, D. Riedel, S. Väth, F. Fuchs, A. Sperlich, P.G. Baranov, V. Dyakonov, G.V. Astakhov. Nature Physics, **10**, 157 (2013).

[6] N.T. Bagraev, V.A. Mashkov, E.Yu. Danilovsky, W. Gehlhoff, D.S. Gets, L.E. Klyachkin, A.A. Kudryavtsev, R.V. Kuzmin, A.M. Malyarenko, V.V. Romanov. Appl. Magn. Resonance, **39**, 113 (2010).

[7] N.T. Bagraev, A.A. Gippius, L.E. Klyachkin, A.M. Malyarenko. Mater. Sci. Forum, **258−263**, 1833 (1997).

[8] N.T. Bagraev, E.Yu. Danilovskii, D.S. Gets, A.K. Kaveev, L.E. Klyachkin, G.I. Kropotov, A.A. Kudryavtsev, R.V. Kuzmin, A.M. Malyarenko, V.A. Mashkov, I.A. Tsibizov, D.I. Tsypishka, I.A. Vinerov. J. Phys.: Conf. Series, **486**, 01 201 (2014).

[9] N.T. Bagraev, A.D. Bouravleuv, L.E. Klyachkin, A.M. Malyarenko, W. Gehlhoff, V.K. Ivanov, I.A. Shelykh. Semiconductors, **36**, 462 (2002).

[10] A. Slaoui, E. Fogarassy, J.C. Muller, P. Siffert. J. Phys. Colloq. C5, **44**, 65 (1983).

[11] N.T. Bagraev, W. Gehlhoff, L.E. Klyachkin. Sol. St. Phenomena, **47−48**, 589 (1995).

[12] N.T. Bagraev, N.G. Galkin, W. Gehlhoff, L.E. Klyachkin, A.M. Malyarenko. J. Phys.: Condens. Matter, **20**, 164 202 (2008).

[13] J.P. Reithmaier, G. Sek, A. Loffler, C. Hofmann, S. Kuhn, S. Reitzenstein, L.V. Keldysh, V.D. Kulakovskii, T.L. Reinecke, A. Forchel. Nature, **432**, 197 (2004).

[14] P.G. Baranov, A.P. Bundakova, A.A. Soltamova, S.B. Orlinskii, I.V. Borovykh, R. Zondervan, R. Verberk, J. Schmidt. Phys. Rev. B, **83**, 125 203 (2011).

[15] C.J. Cochrane, P.M. Lenahan, A.J. Lelis. Appl. Phys. Lett., **102**, 193 507 (2013).

[16] P.G. Baranov. Def. Diff. Forum, **148-149**, 129 (1997).

[17] X.-F. He, N.B. Manson, P.T.H. Fisk. Phys. Rev. B, **47**, 8816 (2000).

[18] M.V. Muzafarova, I.V. Ilyin, E.N. Mokhov, V.I. Sankin, P.G. Baranov. Mater. Sci. Forum, **527-529**, 555 (2006).

Редактор Л.В. Шаронова